
Article:
Phadtare, JA, Fletcher, JK, Ross, AN orcid.org/0000-0002-8631-3512 et al. (2 more authors) (2022) Froude-number-based rainfall regimes over the Western Ghats mountains of India. Quarterly Journal of the Royal Meteorological Society, 148 (748). pp. 3388-3405. ISSN 0035-9009

https://doi.org/10.1002/qj.4367

ORIGINAL ARTICLE

Journal Section

Froude number-based Rainfall Regimes over the Western Ghats Mountains of India

Jayesh A. Phadtare[1,2*] | Jennifer K. Fletcher[1,2] | Andrew N. Ross[1] | Andrew G. Turner[3,4] | Reinhard K. H. Schiemann[4]

[1]School of Earth and Environment, University of Leeds, UK

[2]National Centre for Atmospheric Science, University of Leeds, UK

[3]Department of Meteorology, University of Reading, UK

[4]National Centre for Atmospheric Science, University of Reading, UK

Correspondence
Jayesh Phadtare, Department of Civil and Environmental Engineering and Earth Sciences, University of Notre Dame, Notre Dame, IN 46556
Email: jayesh.phadtare@gmail.com

Present address
[*]Department of Civil and Environmental Engineering and Earth Sciences, University of Notre Dame, Notre Dame, IN 46556

Funding information
This work and its contributors (JAP, JKF, ANR, AGT, RKHS) were funded through the Weather and Climate Science for Service Partnership (WCSSP) India, a collaborative initiative between the Met Office, supported by the UK Government's Newton Fund, and the Indian Ministry of Earth Sciences (MoES).

The variations in the character of monsoonal rainfall over the Western Ghats region on the west coast of India are studied using radiosondes, satellite observations and reanalysis products. Summer monsoon rainfall over this region occurs in alternate offshore and onshore phases. It is shown that these phases are primarily controlled by the strength of the low-level westerly jet. Thus, a classification based on the Froude number, F = U/NH, of the onshore flow is proposed, where, H is the mountain height, U is the mean wind speed and N is the mean Brunt-Väisäla frequency over depth H. At low F (< 0.5), onshore winds are weak and the diurnal thermal fluctuation over the orography is strong; the land-sea and mountain-valley circulations are enhanced leading to a stronger diurnal control over the rainfall. A nocturnal offshore propagation of rainfall from the west coast is seen during this phase. Rainfall over the rainshadow region to the east of the Western Ghats also increases due to a weaker lee effect while it decreases over the Western Ghats due to a greater blocking effect. At high F (> 1), the orographic blocking of the low-level winds is weak. Thus, rainfall is enhanced over the Western Ghats and reduced over the rainshadow region due to a stronger lee effect. In this phase, the diurnal thermal fluctuation over the orog-

raphy is weak. The bulk Richardson number is less than 1 suggesting a dominance of vertical wind shear over the buoyancy forces. The level of free convection and convective inhibition over the west coast are also very low. Hence, at high F, rainfall over the west coast mainly results from the mechanical uplifting of the westerly winds by the Western Ghats with no preference to a particular time of the day. These findings will help in improving the representation of orographic effects and the diurnal cycle of rainfall in numerical models.

KEYWORDS
Flow over orography, Land-sea/Mountain-valley circulation, Indian monsoon, Coastal meteorology.

1 | INTRODUCTION

The Western Ghats is a mountain escarpment running parallel to the west coast of India. Its average elevation is around 800 m, with some of the peaks rising above 1000 m, sloping down eastward to a plateau over the central southern peninsula (Figure 1a). During the summer monsoon season (June-September), a moisture-laden westerly jet impinges on the Western Ghats. As a result, the west coast of India accumulates very high rainfall during this period (Figure 1b,c). The influence of the Western Ghats on the Indian monsoon has been a topic of research for several decades (Grossman and Durran, 1984; Smith, 1985; Xie et al., 2006; Arushi et al., 2017). Although 'flow over an orographic barrier' has been a canonical problem in fluid mechanics and simple theories have been proposed (Queney, 1948; Sheppard, 1956; Smith, 1979; Hunt and Snyder, 1980; Pierrehumbert and Wyman, 1985), its application to real-world cross-orographic flows and the resulting convection has limitations due to the diabatic effects (diurnal and latent), influence of synoptic weather disturbances and the paucity of relevant observations in mountainous terrains.

Based on an energy conservation argument by Sheppard (1956), the criterion for orographic flow blocking can be given by a non-dimensional Froude number (F):

$$F = \frac{U}{NH} \tag{1}$$

where H is height of the orography, U is the mean wind speed across the mountain barrier and N is the mean Brunt-Väisäla frequency of the atmosphere. Mean values of U and N in a layer of depth H from the surface are generally considered for calculating F (Jiang, 2003). N is a measure of the stratification of atmosphere:

$$N = \left[\frac{g}{\theta_v}\frac{\partial \theta_v}{\partial z}\right]^{\frac{1}{2}} \tag{2}$$

$$\theta_v = \theta(1 + 0.61r - r_L) \tag{3}$$

where θ_v is virtual potential temperature, θ is potential temperature, r is the mixing ratio of the water vapor and r_L is the mixing ratio of liquid water in the air. F, essentially, reflects a relative dominance of kinetic energy and stratification of winds across the orography [1]. When $F < F_{critical}$, flow is blocked and deflected by the orography; when $F > F_{critical}$, the flow overcomes the orographic barrier and moves to the leeward side (Sheppard, 1956; Hunt and Snyder, 1980; Smith, 1980; Smith and Grønås, 1993; Baines and Smith, 1993; Jiang, 2003). When the pressure perturbation due to orography is neglected, $F_{critical} = 1$ (Sheppard, 1956). However, when flow approaches orography, the orography induced pressure perturbation can be significant and $F_{critical}$ can be somewhat greater than 1 (Smith, 1989). Nevertheless, $F_{critical} = 1$ can be assumed for most practical applications (Baines and Smith, 1993; Jiang, 2003). The ascent of flow over the slopes of orography by virtue of its kinetic energy is generally referred to as 'mechanical uplifting' of winds. In addition to mechanical uplifting, diurnal heating can also cause 'thermal ascent' over the orography whereby an air parcel rises by virtue of its buoyancy. The rainfall distribution over and in the vicinity of orography can be sensitive to the circulations associated with mechanical uplifting and thermal ascent (Nugent et al., 2014; Kirshbaum et al., 2018). Sarker (1966) argues that the heavy rainfall events over the Western Ghats slopes can almost entirely be attributed to mechanical uplifting of monsoonal low-level westerly winds.

However, the rainfall products from satellite algorithms that consider IR brightness temperature for deriving rainfall, falsely locate the summer monsoon rainfall maximum over the west coast of India (Shige et al., 2017). Instead, rain-gauge data shows that the stations over the slopes of Western Ghats get more rainfall compared to the coastal stations during the summer monsoon season (India Meteorological Department, 2015). For example, Agumbe (which records the highest June-September rainfall over peninsular India) at an elevation of 659 m gets on average 6866 mm of rainfall in a season, whereas the nearby coastal station Mangalore (elevation 30 m) receives 3012 mm. Similarly, Mahabaleshwar at an elevation of 1300 m receives 5362 mm and the nearby coastal station Ratnagiri receives 2928 mm. It was suspected that the anvils of deep convective clouds get advected to the west by the upper-level easterlies, giving the false rainfall maximum over the coast in the satellite derived rainfall products. Recent studies, in fact, show that the clouds along the coast are deeper than those over the Ghats (Shrestha et al., 2015; Kumar and Bhat, 2017). Rainfall estimate in the TRMM PR 2A25 dataset, which is derived exclusively from a precipitation radar (PR), shows that the rainfall maximum is indeed over the slopes of Western Ghats (Nesbitt and Anders, 2009; Romatschke and Houze, 2011; Shrestha et al., 2015; Shige et al., 2017). Thus, detailed and accurate observations are a prerequisite for the understanding of orographic effects of the Western Ghats. Such observations can also be useful in the improvement of numerical models (Ogura and Yoshizaki, 1988; Xie et al., 2006; Prabha et al., 2011; Choudhury and Krishnan, 2011; Rajendran et al., 2012; Flynn et al., 2017; Zhang and Smith, 2018).

An offshore-onshore oscillation of rainfall over the west coast of India has been highlighted in some recent studies (Zhang and Smith, 2018; Fletcher et al., 2020; Hunt et al., 2021). The exact mechanism behind this oscillation is not well understood. Grossman and Durran (1984) used a 2D analytical model to propose that the offshore rainfall over the Arabian Sea can be a result of the upstream blocking by the Western Ghats. However, their model did not account for planetary rotation and latent heat effects (Smith, 1985). In a dry 2D hydrostatic flow, planetary rotation puts a length-scale constraint on the upstream orographic influence (Pierrehumbert and Wyman, 1985). Latent heat effects associated with convection alter the stratification along the orography, and hence, affect the orographic blocking (Miglietta and Buzzi, 2001; Jiang, 2003; Chen and Lin, 2005; Reeves and Lin, 2007; Phadtare, 2018). Ogura and Yoshizaki (1988) showed, using a 2D cloud model, that latent heat effects, vertical wind shear, and surface fluxes are necessary to simulate the correct location of the observed rainfall over the west coast of India. By performing WRF

[1] Some literature (e.g., Smith (1989)) prefer using the term 'non-dimensional mountain height', $h = NH/U$, as the fluid mechanics community perceives the term 'Froude number' as the ratio of fluid speed to gravity wave speed. We will stick to the term 'Froude number' since its use as a measure of orographic flow blocking is quite prevalent in the meteorological community.

model simulations, Zhang and Smith (2018) suggested that the offshore rainfall is associated with high Arabian Sea SST and dry mid-tropospheric layer; they also argue that the Western Ghats do not trigger the offshore convection. Fletcher et al. (2020) observed a transition from a regime of widespread offshore rainfall to a regime of rainfall primarily on the coast and windward slopes of the Western Ghats during an intensive field campaign. They argued that the shift from offshore to onshore rainfall was controlled primarily by the mid-tropospheric humidity and the strength and humidity of the low-level westerlies, which themselves evolved in response to the large-scale circulation. This conclusion was confirmed in a climatological study by Hunt et al. (2021). They found that the second empirical orthogonal function of rainfall over the coastal region was one of offshore/onshore rainfall modes, and these modes were associated with wind and thermodynamic profiles similar to those seen by Fletcher et al. (2020). Francis and Gadgil (2006) suggest that the offshore rainfall over the west coast is linked to planetary scale atmospheric signals over the equatorial Indian Ocean. Shige et al. (2017) show that offshore rainfall is preferred during the 3rd and 4th phases of Boreal Summer IntraSeasonal Oscillation (BSISO) while onshore rainfall is preferred during the 5th and 6th phases. They attribute the offshore-to-onshore transition to enhancement of the westerly winds alone.

Variations in upstream rainfall accumulations with the Froude number of the impinging flow have been reported in idealised modelling studies (Chu and Lin, 2000; Reeves and Lin, 2007; Miglietta and Rotunno, 2009). Fletcher et al. (2020) computed the Froude number of the flow using aircraft data in their observed offshore and onshore regimes and found that the Froude number did not vary much between the regimes. They thus concluded that the mid-tropospheric humidity exerted a greater control on the spatial distribution of rainfall. However, this computation was only done for a limited time period and at different times of day. Winds and stratification can vary significantly during the course of day.

A systematic documentation of how the intensity and diurnal cycle of rainfall over the Western Ghats region vary with the strength of monsoonal lower-tropospheric westerly flow is missing in the scientific literature. Thus, the primary objective of this study is to understand how interactions between the monsoon westerly flow and land-sea/mountain-valley circulations near the Western Ghats lead to different rainfall regimes during the summer monsoon season. In the glossary of the American Meteorological Society, the term 'rainfall regime' is described as 'the character of the seasonal distribution of rainfall' at any place. In different regimes, rainfall characteristics like intensity, diurnal variations, cloud organization, and microphysics can be different.

In this study, we propose a classification of the phases of the low-level westerly winds based on its F values. This classification is able to separate the different rainfall regimes over the Western Ghats. It has a plausible dynamical basis with a bearing on the land-sea/mountain-valley breezes and the diurnal cycle of rainfall. Radiosonde soundings from weather stations over the west coast (Figure 1) are used to calculate F. Section 2 describes the datasets used and the calculation of F. Section 3 puts forth a classification based on the F values of the monsoonal flow for separating the rainfall regimes over the Western Ghats. Sections 4 and 5 describe the variations in the rainfall characteristics (intensity, diurnal variation) and circulation (land-sea, mountain-valley breezes), respectively, over the Western Ghats in the different phases of F. Section 6 concludes the study.

2 | DATA AND METHODS

2.1 | Atmospheric soundings

Radiosonde soundings give in situ vertical profiles of the atmosphere at point locations. This data can have high vertical resolution and is ideal for calculating the stratification of the lower atmosphere. WMO-class weather stations release radiosondes twice per day: at 0000 and 1200 UTC (+0530 IST). Soundings from Mumbai, Goa, Mangalore, Kochi (all

over the west coast), Aminidivi (an island in the Arabian Sea) and Bangalore (in the rainshadow of the Western Ghats) are used in this study. Soundings for the June-September 2000-2018 period were downloaded from the University of Wyoming website (`http://weather.uwyo.edu/upperair/sounding.html`). The locations of the sounding stations are shown on the map in Figure 1a.

2.2 | Rainfall

The precipitation radar (PR) on-board the TRMM satellite gives the most reliable estimation of the instantaneous surface rainfall from space. However, the TRMM 2A25 surface rainfall, which is exclusively derived from PR, is orbital data. This dataset is ideal for describing the meso-α scale (few km) gradients of rainfall over a long-term ($\sim$ decade) but not for a time span of $\sim$ 100 days as well as the diurnal cycle of rainfall. Thus, we have used the Integrated Multi-satellitE Retrievals for GPM (IMERG) product (Huffman et al., 2015) for studying the variation of rainfall over the Western Ghats region with the F values of the low-level flow. IMERG provides global surface rainfall field over a 0.1° spatial grid at 30 minute intervals. IMERG underestimates seasonal rainfall over the Western Ghats escarpment (Figure 1c). Implications of this drawback will be discussed when the results are analysed in section 4. We have also verified the results of this study by repeating the analysis with the rainfall field in the Indian Monsoon Data Assimilation and Analysis (IMDAA) reanalysis (Rani et al., 2021) provided by the National Centre for Medium Range Weather Forecasting (NCMRWF). This dataset is available over a 12-km spatial grid at hourly intervals. IMDAA correctly locates the maximum of rainfall intensity over the Western Ghats escarpment (Figure 1b). However, the diurnal variation of rainfall in the IMDAA dataset is poor – continental rainfall peaks in this dataset around 1200 LST (local solar time) which is early by about 4-6 hours (Figure S2 in the supplemental material). Thus, this dataset is not used for analysing the diurnal variation of rainfall. The rainfall variations with Froude number are similar in these two datasets. The plots of rainfall variation using the IMDAA datasets are included in the supplementary figures.

2.3 | Large-scale fields

The ERA-interim (Dee et al., 2011) reanalysis at 6-hourly intervals and $0.75^\circ \times 0.75^\circ$ horizontal resolution is used to describe the large-scale dynamic and thermodynamic conditions of the atmosphere.

2.4 | Calculation of Froude number

A value of F for each sounding is calculated by using equations 1 - 3. The r_L term is neglected as the effect of condensate loading on the buoyancy of parcels in the lowest 1-km atmospheric layer is one order of magnitude less than the temperature and moisture effects (Jiang, 2003). As the Western Ghats range is oriented almost in the north-south direction, the zonal wind itself is assumed to be the cross-orographic flow. Mean values of U and N are calculated by considering an atmospheric layer between 50 m and the peak height of Western Ghats along the latitude of the sounding station (Figure 2a). Soundings in which data was missing or N^2 values were negative within the orographic layer were excluded from the study. The number of available soundings and the number of soundings used for calculating F are shown in the supplementary Figure S1.

Figure 2 shows distributions of mean values of U, N and F at 0000 and 1200 UTC at the four coastal stations. Figure 2b shows that at Mumbai, Goa, and Mangalore the peak of the layer-mean zonal wind speed distribution is around 1-2 $\mathrm{m\,s^{-1}}$ at 0000 UTC and around 5 $\mathrm{m\,s^{-1}}$ at 1200 UTC with speeds exceeding 15 $\mathrm{m\,s^{-1}}$ on rare occasions. Wind speeds are higher at Kochi compared to other stations – peaking around 6 $\mathrm{m\,s^{-1}}$ at 0000 UTC and 8 $\mathrm{m\,s^{-1}}$ at

1200 UTC with speeds exceeding 20 m s^{-1} on rare occasions. Thus, the diurnal variation of wind speeds is strong at Mumbai, Goa, and Mangalore and weak at Kochi. The N values over the coast often lie between 0.005 to 0.02 s^{-2}. The distributions of N do not differ much between sounding stations. However, N can vary over a broad range at a given location. The 1200 UTC N values tend to be smaller than those at 0000 UTC due to the daytime solar heating of the surface; the diurnal variability in N is more pronounced at Mangalore and least at Goa and Kochi. Thus, due to the higher wind speeds and lower stratification the 1200 UTC F values are higher than the 0000 UTC values at all stations. The peak of the 0000 UTC distribution of F is around 0.2 for Mumbai, Goa, and Mangalore and that for Kochi is around 0.8. This is due to the high nocturnal wind speeds at Kochi compared to other stations. The peak of the daytime distribution of F at Kochi is quite close to 1, that at Mumbai and Goa is around 0.8. F values are generally lowest at Mangalore due to weak winds and taller mountains to its east. Both U and N contribute significantly to the variability of F – the correlation coefficient between F and U is around 0.8 and that between F and N is around -0.5.

3 | CLASSIFICATION OF WIND FORCING

The aim of this section is to identify the primary driving factors behind the offshore-onshore oscillation of rainfall over the west coast of India during the summer monsoon season. Based on this, a classification of relevant meteorological parameters is also proposed to predict the rainfall mode.

3.1 | Offshore-onshore rainfall modes

The offshore rainfall mode is characterised by weaker lower-tropospheric westerlies and higher mid-tropospheric humidity, whereas the onshore rainfall mode over the west coast is characterized by stronger lower-tropospheric westerlies and lower mid-tropospheric humidity (Fletcher et al., 2020; Hunt et al., 2021). Here we examine how the rainfall field, in general, responds to the to the individual humidity and winds forcings. Soundings from Aminidivi are used to cluster different phases of mid-tropospheric humidity. A station in the open Arabian Sea is selected as the maximum of the mid-tropospheric humidity anomalies associated with this rainfall oscillation is located over the offshore region (Hunt et al., 2021). Soundings from Mangalore are used to cluster different phases of low-level westerlies. A zonal belt over the Aminidivi-Mangalore region was the focus of Fletcher et al. (2020) and Hunt et al. (2021).

In order to classify the different phases of mid-tropospheric humidity forcing, we consider the dewpoint depression, i.e., difference between the dry bulb and dewpoint temperatures, in the atmospheric layer between 4000-7000 m (at every 1000 m) from the 0000 UTC soundings at Aminidivi. Soundings are clustered in three clusters using the k-means unsupervised clustering algorithm. Three clusters are chosen in order to allow for the moist, dry, and intermediate mid-tropospheric humidity conditions. Similarly, in order to classify the different phases of low-level wind forcing, we take zonal velocities in the atmospheric layer between 500-5000 m (at 500 m and then at every 1000 m) from the 0000 UTC sounding at Mangalore. Soundings are clustered in three clusters according to these wind speeds using the k-means unsupervised clustering algorithm. Three cluster are chosen to allow for strong, weak, and intermediate wind speed conditions.

Figure 3 shows the three clusters of mid-tropospheric humidity (Fig. 3a) and the lower-tropospheric wind speeds (Fig. 3b). In Figure 3a, Cluster 1 contains days featuring a moist mid-troposphere whereas cluster 2 features a dry mid-troposphere. Note that the clustering takes into account the dew point depression values at 4000, 5000, 6000, and 7000 m; only values at 4000 m and 7000 m are shown for the sake of simplicity. Similarly, cluster 0 in Figure 3b

contains days with weak zonal winds and cluster 1 contains days with strong zonal winds. Only speeds at 500 and 5000 m are shown for the sake of simplicity. Note that most of the points lie on the diagonal so there is little variation in the vertical shear in different clusters as far as the lower troposphere is concerned.

Figure 4 shows composite rainfall anomalies in IMERG for the mid-tropospheric humidity and lower-tropospheric wind speed clusters shown in Figure 3. Figure 4a shows that rainfall over the entire region increases when the mid-troposphere is moist and vice-versa. The offshore-onshore rainfall oscillation is not seen with the mid-tropospheric humidity forcing alone. On the other hand, manifestation of the offshore-onshore rainfall dipole is seen with the lower-tropospheric wind forcing exclusively. This implies that the variability in the monsoonal westerly winds is primarily responsible for producing the offshore-onshore rainfall dipole. The mid-tropospheric humidity might play a role in further amplifying this dipole.

Similar rainfall variations in the vicinity of orography with the cross-orographic winds have been reported in idealised simulation experiments (Chu and Lin, 2000; Reeves and Lin, 2007; Miglietta and Rotunno, 2009). These studies show that at $F < 1$, rainfall propagates upstream from the orography, creating a broad region of upstream rainfall accumulation. At $F > 1$, rainfall intensity increases sharply over the windward orographic slopes and it reduces elsewhere in the upstream region. Therefore, next we analyze how F of the low-level monsoonal flow influences rainfall over the Western Ghats and the west coast of India.

3.2 | Phases of F

The 0000 UTC soundings are used to classify the different phases of F. The 0000 UTC sounding are chosen for the following reasons. The peak of the diurnal cycle of rainfall over the Western Ghats is around 1030 UTC (1600 LST) (Flynn et al., 2017; Krishna et al., 2021), thus, the 1200 UTC soundings, on most days, will reflect the conditions over the coast shortly after the peak rainfall events. Secondly, we believe that the nocturnal to early morning anomalous land/valley breeze is a key element in the offshore propagation of rainfall. The background westerly monsoonal flow will always assist the up-slope circulation and hence, onshore/orographic rainfall. Hence, capturing the events when the onshore flow is weakest (or orographic blocking is the strongest) in the day, allowing offshore rainfall, is crucial. This is likely to happen in the night and morning hours. Lastly, the number of 1200 UTC soundings is also fewer than the 0000 UTC soundings at the coastal stations (Figure S1 in the supplemental material) as the 0000 UTC launch is preferred whenever there is a shortage of resources.

We classify F in to the following three categories – (1) Low: $F \leq 0.5$, (2) Moderate: $0.5 < F \leq 1$, and (3) High: $F > 1$. Note that the critical value of F lies around 1. However, we avoid using terms like 'blocked' or 'unblocked' for these phases for the following reasons. Firstly, latent heat release from condensation and evaporation can alter the F values during a convective episode (Jiang, 2003; Reeves and Lin, 2007; Phadtare, 2018). Secondly, F values cannot be accurately measured in the precipitating environment – away[2]. from the orography (where F should ideally be calculated), the stratification can be different from that near the orography (Phadtare, 2018); and near the orography, flow is already under the influence of pressure perturbations from orography (Markowski and Richardson, 2011). Nevertheless, in the Low F phase, the flow is most likely to be strongly blocked and in the High F phase, the flow is most likely weakly blocked by the Western Ghats. Next, we show how the rainfall and circulation regimes differ in the different phases of F.

[2]The term 'away' implies at a distance more than the orographic radius of deformation, $R_d = NH/f$, where f is the Coriolis parameter (Pierrehumbert and Wyman, 1985). This is the width of the flow deceleration zone from the orography. For the Western Ghats, $R_d \sim$ 150 km - 300 km

4 | RAINFALL REGIMES

Previous studies defined the offshore and onshore modes of rainfall by considering rainfall intensities over the respective regions (Zhang and Smith, 2018; Fletcher et al., 2020; Hunt et al., 2021). Here we are trying to identify the changes in the rainfall pattern in different flow regimes defined in terms of relevant flow parameters such as F, and determine whether these rainfall regimes are related to the rainfall modes identified previously. We use the term rainfall regimes to differentiate from the term 'rainfall modes' used by Hunt et al. (2021) for the phases of rainfall based on its intensity. This section describes the rainfall regimes associated with the different phases of F.

4.1 | Spatial distribution

Figure 5a shows rainfall anomalies from the IMERG dataset for the three phases of F derived from the soundings at Mangalore. It shows that for Low F, rainfall anomalies over the Western Ghats are uniformly negative, and over the adjacent Arabian Sea, the anomalies are uniformly positive. The opposite happens during the High F phase. Thus, the classification of phases of westerly monsoonal flow according to the F values captures the offshore-onshore regimes of rainfall. Rainfall anomalies over the rainshadow region to the east of the Western Ghats are out of phase with the onshore rainfall anomalies. This is due to variations in the strength of the lee-effect of the Western Ghats in different F phases – stronger in high F phase and vice-versa. Note that for Moderate F, weak positive rainfall anomalies lie over the coast. Thus, this classification leads to regimes of precipitation that follow the topography more closely compared to the unsupervised clustering classification described in section 3.1 (Figures 3b and 4b). This is expected as the clustering technique has a purely statistical underpinning, whereas the Froude number-based classification follows physical reasoning and takes into account variations in the stability as well as wind speed. Physically, both are important in determining the regime. Figure 5b shows the contribution of different phases of F to the total seasonal rainfall accumulation. The rainshadow region of the Western Ghats and the western Arabian Sea get more than 70% of its seasonal rainfall from the Low F phase. The coastal region has nearly equal contributions from all three phases. The High F phase covers just about 10% of the total period and contributes to about 50% of the total rainfall over the Western Ghats, another 30-40% comes in the Moderate F phase and the Low F contributes about 10-20%.

Similar results are seen when soundings at Mumbai, Goa, and Kochi are considered (Figure S3 in the supplementary material). Figure 6 shows the meridionally averaged intensities of rainfall over the 1° zonal belt centred at the latitudes of Mumbai, Goa, Mangalore, and Kochi in the different phases of F derived from the soundings at the respective stations. In the High F phase, rainfall intensity has a sharp peak over the Western Ghats slopes, evident using any of the stations. In the Low F phase, rainfall intensity decreases drastically over the Western Ghats and increases over a large area of the Arabian Sea. The maximum rainfall in this phase occurs along the coast. Similar rainfall variations over the upstream region and orography were reported by varying the F values of impinging flow in the idealised simulations (Chu and Lin, 2000; Reeves and Lin, 2007). Note that the IMERG product underestimates the seasonal rainfall accumulation over the Western Ghats slopes and how the bias varies in the different rainfall regimes is unclear at this point. Figure S4 in the supplementary material shows that the rainfall anomalies for the different phases of F using the IMDAA dataset are similar to those generated using IMERG.

4.2 | Diurnal variation

Figure 7a shows a spatial map of the peak timing of the mean diurnal cycle of rainfall during the three phases of F using the IMERG dataset. These phases are derived from the soundings at the Mangalore upper-air station. The Low F

phase is characterised by regions with similar peak hours of the diurnal cycle of rainfall. These regions are setup by the topography. During the Low F phase, there is a clear land-sea contrast along the west coast in the hour of maximum rainfall intensity. Over the coastal land, the rainfall intensity is a maximum at 1600 LST whereas over the sea it is at 0000 LST. Over the Western Ghats peaks, rainfall intensity is maximum at 1600 LST and over the rainshadow, it is at 0000 LST. The separation between these two regions is quite stark and it runs parallel to the Western Ghats range. A nocturnal upwind phase propagation over the west coast is also seen as the hour of maximum intensity changes gradually from 0000 LST along the coast to 0900 LST over the open sea. The spatial scale of this gradient suggests that the speed of propagation of the line of maximum rainfall is around 8-10 $\mathrm{m\,s^{-1}}$. In the High F phase, there is no clear land-sea contrast in the hour of maximum rainfall over the west coast. There is high spatial variation in the hours of maximum rainfall over the peninsula and homogeneous regions are not present. The rainfall peaks over the rainshadow region later in the day (1600 - 0000 LST), whereas over the west coast and Western Ghats, nocturnal to early morning hours (0000-1000 LST) are most likely to receive heavy rainfall.

The conventional statistical measures are not appropriate for describing the distribution of angular quantities such as 'LST' . Thus, circular standard deviation (σ_c), as described by Fisher (1995), will be used here as a measure of the variation of hour of maximum rainfall. Figure 7b shows σ_c of the hour maximum rainfall on each day over the region in the different phases of F, with low values indicating a narrow peak that is tightly confined to a particular time of day. Only rainfall intensities greater than 1 mm/hour are considered. During the Low F phase, σ_c is around 2-4 hours over the rainshadow region, over the coast it is around 6-8 hours and over the offshore region it is around 5-6 hours. The lower values of σ_c over the rainshadow region imply that the diurnal variation of rainfall is closely tied to the solar heating of the land, whereas higher values of σ_c over the coast imply that the rainfall here gets significant assistance from the mechanical uplifting of the winds by the Western Ghats. During the High F phase, the σ_c over a large part of the Indian peninsula is around 8-12 hours, suggesting the dominant role of mechanical uplifting by the orography, especially over the Western Ghats. In the Moderate F phase, the diurnal variation of rainfall over the west coast is similar to that in the High F phase, whereas over the plateau, it is more like the Low F phase. The diurnal variation in the different phases of F based on the soundings at Mumbai, Goa and Kochi are also similar (Figure S5 in the supplementary material).

5 | DYNAMICS AND THERMODYNAMICS OF RAINFALL REGIMES

Large-scale variability is responsible for the variation in strength of the westerly winds across the west coast of India (Shige et al., 2017), and hence, its F values. The different phases of F have different regimes of atmospheric circulation over orography. This section shows that the observed rainfall regimes are coherent with the different regimes of circulation like land-sea and mountain-valley breezes.

5.1 | Large-scale circulation

Figure 8 shows the large-scale 800 hPa winds during the different phases of F based on Mangalore soundings. During the Low F phase, the monsoonal jet is weak and the trough over the core monsoon zone (north Bay of Bengal and central India) is also absent. During the Moderate and High F phases, the monsoon trough and the westerly flow are quite strong – much stronger during the High F phase. Thus, the Moderate and High F phases are more likely when a low pressure system (LPS) is present over the core monsoon zone. Figure 9 shows that F is generally high during the BSISO phases 5-7 and it is generally low during phases 2-4. Shige et al. (2017) reported that the onshore rainfall

follows the northward moving vortices which accelerate the westerly winds to its south during the BSISO phases 4-6. Next, we analyze how the land-sea/mountain-valley type of circulation over the Western Ghats responds to the diurnal heating of the orography during the different phases of *F*.

5.2 | Land-sea and mountain-valley breezes

Figure 10 shows distributions of mean wind direction in a layer between 50-1000 m (Φ_{oro}) and 2000-3000 m ($\Phi_{2-3\text{km}}$) in the Mangalore soundings at 0000 and 1200 UTC. In the Low *F* phase, the peak of the 0000 UTC Φ_{oro} distribution is around 200°, i.e., southerly, whereas the peak of the 1200 UTC Φ_{oro} distribution is around 300 °, i.e., northwesterly. The peak of the $\Phi_{2-3\text{km}}$ distribution is in the westerly direction and there are no significant changes in the distribution with the timing of soundings. Thus, during the Low *F* phase, we see the low-level westerly winds getting deflected to assume southerly directions in the nighttime and northwesterly in the daytime. Rotation of winds with solar heating and nighttime cooling were also reported by Prabha et al. (2011) in the lee-side of the Western Ghats and by Hindman (1973) in the Redwood Creek Valley in California.

During the high *F* phase, the peaks of both Φ_{oro} and $\Phi_{2-3\text{km}}$ distributions are at 270°. Thus, during the high *F* phase, winds flow towards the orographic slopes undeflected. During this phase, diurnal variations in the low-level wind direction are also absent. The Φ_{oro} and $\Phi_{2-3\text{km}}$ distributions for the moderate *F* phase are more like the High *F* phase. Similar conclusions can be drawn by analyzing the soundings at Mumbai and Goa. At Kochi, the upper-level winds during the Low *F* phase are northwesterlies (Figure S6 in the supplementary material) and the diurnal rotation of the low-level winds is not so prominent.

Figures 11a-d show the 12°N-14°N meridional mean of the zonal and vertical wind anomalies, and the potential temperature at 0000 and 1200 UTC for the Low and High *F* phases. The wind anomalies are derived by subtracting the mean of the respective phases. Figure 11e shows the difference between the quantities shown in Figures 11a and 11c. Similarly, Figure 11f shows the difference between the quantities in Figures 11b and 11d. During the Low *F* phase, there is more cooling at 0000 UTC and more heating at 1200 UTC over the Western Ghats orography compared to the High *F* phase. The nocturnal cooling of the plateau in the Low *F* phase is probably due to the increase in the rainfall intensity with its peak at 0000 LST/~1830 UTC (Figures 6c and 7a). The cooling of the Western Ghats could be due to the enhanced katabatic winds at that time. The day-time heating of the plateau in the Low *F* phase could be due to the delayed rainfall and reduced wind-induced ventilation (Nugent et al., 2014). Cloud radiative effects might also be important for the observed diurnal heating differences. The relative contribution of different factors in the diurnal thermal fluctuation of the Western Ghats topography could be looked at in detail in the future studies. During the Low *F* phase, there is a pronounced anomalous valley breeze in the night-time and anomalous mountain breeze in the day-time on the slopes of the Western Ghats. This results in strong anomalous day-time convergence and night-time divergence over the plateau. With the help of a WRF simulation, Prabha et al. (2011) have shown that when Froude number of the flow is less than 1, the temperature difference between the valley and Western Ghats slopes can reach up to 14 K. This strong temperature gradient drives the nocturnal boundary layer jet on the lee-side. During the High *F* phase, the mountain-valley type of circulation is absent over the Western Ghats.

In summary, during the Low *F* phase, thermal forcing from the topography and the land-sea/mountain-valley types of circulations over the west coast seem to play an important role in controlling the rainfall over this region. During the High *F* phase, the thermal forcing by the Western Ghats topography is very weak and the onshore flow is strong. Hence, the land-sea and mountain-valley type of circulations are very weak in this phase. Consequences of strong and weak land-sea/mountain-valley circulations in the Low and High *F* phases, respectively, were seen in the diurnal pattern of rainfall in section 4.2 (Figure 7).

5.3 | Shear instability

In a stably stratified fluid, the buoyancy suppresses vertical motion whereas the vertical shear tends to promote turbulent motion and vertical mixing. The relative dominance between the two can be determined from the bulk Richardson number (e.g., Richardson et al. (2013)):

$$Ri_b = \frac{g}{\theta_v} \frac{\Delta\theta_v \Delta Z}{(\Delta u)^2 + (\Delta v)^2} \tag{4}$$

where, ΔZ is the thickness of the fluid layer and Δu and Δv are zonal and meridional wind shear over the layer. High Ri_b values suggest strong stratification and less vertical mixing. From equations 1 and 4, the following relationship between between the Froude and Richardson numbers can be derived using dimensional similarity:

$$Ri_b = 1/F^2 \tag{5}$$

Here, we take ΔZ as the layer thickness between 50 m and the mountain top (1000 m) and calculate Ri_b using observations from the 0000 UTC Mangalore soundings and equation 4. Figure 12a shows the scatter of Ri_b versus F. The scatter follows the theoretical curve given by equation 5. In low F regime, Ri_b values greater than 1 are quite numerous. As F increases Ri_b falls sharply and it is generally below 1 in the high F regime. The critical value of Ri_b below which the fluid becomes turbulent is not well defined. However, the literature suggest that it lies between 0.2-1 (Galperin et al., 2007). The drop in Ri_b at high F is due to low atmospheric stability (Figure 12a) as well as high wind shear (Figure 12b).

5.4 | Thermodynamic instability

Figure 13 shows the composite 0000 and 1200 UTC soundings at Mangalore (over the west cost) and Bangalore (over the plateau at an elevation of 900 m) during the High and Low F phases. The conditions seen in Figure 11 are roughly echoed by the soundings; in the Low F phase, the plateau is warmer at 1200 UTC and the inversion is stronger over the coast at 0000 UTC.

Figure 14 shows mean values of the level of free convection (LFC), level of neutral buoyancy (LNB), convective available potential energy (CAPE), and convective inhibition (CIN) from the soundings at Mangalore and Bangalore during the Low and High F phases. During the High F phase, the LFC and CIN are lower and CAPE and LNB are higher over Mangalore. Thus, the conditions at Mangalore are more favourable for deep convection during the High F phase. Note that the mean LFC during the High F phase, is roughly at the level of the mountain height near Mangalore, whereas the mean LFC during the Low F phase is near to 800 hPa. Thus, the release of convective instability purely by orographic uplifting is more likely over the coast during the High F phase. Over Bangalore, the LFC is lower and CAPE is higher during the Low F phase. Thus, the conditions at Bangalore are more favourable for deep convection during the Low F phase. Note that greater plateau heating during the Low F phase is reflected in the daytime mean sounding at Bangalore, however, the mean moisture profiles in the lower troposphere do not vary much between the different phases (Figure 13b). Over Mangalore, the surface conditions are more moist as well as warm during the High F phase (Figure 13a). Thus, the greater amount of instability at the coast during the High F phase can mainly be attributed to the advection of warm and moist air by the stronger westerly flow, whereas over the plateau, the rise in

instability is mainly due to the daytime heating.

There is some diurnal variability in the thermodynamic conditions at Bangalore, especially during the High F phase. The CAPE at Mangalore dose not vary much diurnally. However, there is a sharp fall in the CIN in the nighttime during the High F phase. The processes that lead to this fall are unclear at this point.

6 | CONCLUSIONS AND DISCUSSION

During the summer monsoon season, rainfall over the west coast of India occurs in the offshore and onshore phases. Earlier studies had reported that the offshore phase is characterised by a moist mid-troposphere and weak lower-tropospheric westerlies, while the opposite is true for the onshore phases. This study shows that the lower-tropospheric wind variability is the main forcing mechanism for the offshore-onshore dipole of rainfall. The salient aspect of the clustering method used in section 3.1 is that the rainfall field was not constrained to evolve in a particular fashion. The clusters solely involving the mid-tropospheric humidity variability did not lead to an offshore-onshore dipole of rainfall, whereas those with the lower-tropospheric zonal winds did. Classification of the low-level monsoonal flow on the basis of Froude number (F) led to different rainfall regimes over the Western Ghats. In the Low F phase, there is a greater blocking of the flow by the Western Ghats; hence, rainfall over the west coast and the Ghats reduces. The daytime heating and nighttime cooling of the Western Ghats give stronger land-sea and mountain-valley breezes during this phase – the coastal breeze in daytime is northwesterly while in the early morning it is southerly. Thus, the diurnal cycle of rainfall is also strong. Rainfall over the plateau increases during this phase due to the convergence caused by the daytime anomalous mountain breeze while in the nocturnal hours, rainfall propagates offshore from the west coast. During the High F phase, the offshore propagation of rainfall is absent, rainfall increases sharply over the slopes of the Western Ghats. The bulk Richardson number of the flow approaching the Western Ghats is generally less than 1 during this phase. This suggests a dominance of vertical wind shear over stratification, and hence, a propensity towards turbulence. In addition, the LFC along the west coast is lowered down roughly to the mountain height. Hence, rainfall mainly results from the mechanical uplifting of the monsoonal jet. Thus, the diurnal cycle of rainfall is weak during this phase. The schematic in Figure 15 summarizes the findings of this study.

In their idealised model experiments, Chu and Lin (2000) showed that when convection was already present in the far upstream region, rainfall over the orographic slopes was suppressed by the cold air outflows from the upstream region. A similar observation was made by Fletcher et al. (2020) over the west coast of India. Such cold air outflows may manifest as Low F flows over the coast as these flows are highly stratified. Thus, the convective downdrafts and surface cold pools can be an important element of the offshore-onshore rainfall oscillation. The offshore convection can be triggered independently by a large-scale weather system (Shige et al., 2017) or by orographic blocking along the coast which subsequently propagates offshore.

In idealised modelling experiments, storms continuously propagate in the upwind direction when the F values are low, while in the high F case, storms are stationary over the upwind slopes of the orography (Chu and Lin, 2000; Reeves and Lin, 2007; Miglietta and Rotunno, 2009). The upwind convergence caused by the gust front is believed to be the mechanism behind the offshore propagation of rainfall in these idealised simulations. Similar behaviour of storms can be expected over the west coast of India as well; the nocturnal offshore propagation of rainfall during the Low F phase hints at this possibility. Propagation of individual storms could be studied using a ground-based radar over the west coast to understand how the strength of low-level flow affects storm propagation.

Diurnal effects were not present in these idealised modelling experiments. Mapes et al. (2003) performed a model simulation of a real world case-study over the Colombia coast in South America to study the nocturnal offshore

propagation of rainfall. They showed that the nocturnal offshore rainfall propagation is tied to the diurnal gravity wave generated by the elevated terrain. The topographical setting of the west coast of India is ideal for such diurnal gravity wave generation, especially in the Low F phase that features greater diurnal thermal fluctuation of the plateau and weaker onshore winds. Thus, in a follow up study we plan to investigate the role of the Western Ghats in the offshore-onshore rainfall modes. We will use a regional model and perform several sensitivity tests to understand the impact of model resolution and convective parameterization on the offshore-onshore rainfall modes over the west coast. If the interaction between cloud- and large-scale is vital, faithful simulation of the rainfall modes could be a challenging task for the convective parameterization schemes.

acknowledgements

This work and its contributors (JAP, JKF, ANR, AGT, RKHS) were funded through the Weather and Climate Science for Service Partnership (WCSSP) India, a collaborative initiative between the Met Office, supported by the UK Government's Newton Fund, and the Indian Ministry of Earth Sciences (MoES). Authors also gratefully acknowledge NCMRWF, Ministry of Earth Sciences, Government of India, for IMDAA reanalysis. IMDAA reanalysis was produced under the collaboration between UK Met Office, NCMRWF, and IMD with financial support from the Ministry of Earth Sciences, under the National Monsoon Mission programme. JAP thanks Thorwald H.M. Stein and Kieran M.R. Hunt at the University of Reading for their constructive comments on this study.

references

Arushi, P., Chakraborty, A. and Nanjundiah, R. S. (2017) Orographic control of the Bay of Bengal cold pool rainfall. *Journal of Earth System Science*, **126**, 1–16.

Baines, P. G. and Smith, R. B. (1993) Upstream stagnation points in stratified flow past obstacles. *Dynamics of Atmospheres and Oceans*, **18**, 105–113.

Chen, S.-H. and Lin, Y.-L. (2005) Effects of moist Froude number and CAPE on a conditionally unstable flow over a mesoscale mountain ridge. *Journal of the Atmospheric Sciences*, **62**, 331–350.

Choudhury, A. D. and Krishnan, R. (2011) Dynamical response of the South Asian monsoon trough to latent heating from stratiform and convective precipitation. *Journal of the Atmospheric Sciences*, **68**, 1347–1363.

Chu, C.-M. and Lin, Y.-L. (2000) Effects of orography on the generation and propagation of mesoscale convective systems in a two-dimensional conditionally unstable flow. *Journal of the Atmospheric Sciences*, **57**, 3817–3837.

Dee, D. P., Uppala, S., Simmons, A., Berrisford, P., Poli, P., Kobayashi, S., Andrae, U., Balmaseda, M., Balsamo, G., Bauer, d. P. et al. (2011) The ERA-Interim reanalysis: Configuration and performance of the data assimilation system. *Quarterly Journal of the Royal Meteorological Society*, **137**, 553–597.

Fisher, N. I. (1995) *Statistical analysis of circular data*. Cambridge University Press.

Fletcher, J. K., Parker, D. J., Turner, A. G., Menon, A., Martin, G. M., Birch, C. E., Mitra, A. K., Mrudula, G., Hunt, K. M., Taylor, C. M. et al. (2020) The dynamic and thermodynamic structure of the monsoon over southern India: New observations from the INCOMPASS IOP. *Quarterly Journal of the Royal Meteorological Society*, **146**, 2867–2890.

Flynn, W. J., Nesbitt, S. W., Anders, A. M. and Garg, P. (2017) Mesoscale precipitation characteristics near the Western Ghats during the Indian Summer Monsoon as simulated by a high-resolution regional model. *Quarterly Journal of the Royal Meteorological Society*, **143**, 3070–3084.

Francis, P. and Gadgil, S. (2006) Intense rainfall events over the west coast of India. *Meteorology and Atmospheric Physics*, **94**, 27–42.

Galperin, B., Sukoriansky, S. and Anderson, P. S. (2007) On the critical Richardson number in stably stratified turbulence. *Atmospheric Science Letters*, **8**, 65–69.

Grossman, R. L. and Durran, D. R. (1984) Interaction of low-level flow with the Western Ghat mountains and offshore convection in the summer monsoon. *Monthly Weather Review*, **112**, 652–672.

Hindman, E. E. (1973) Air currents in a mountain valley deduced from the breakup of a stratus deck. *Monthly Weather Review*, **101**, 195–200.

Huffman, G. J., Bolvin, D. T., Nelkin, E. J. and Tan, J. (2015) Integrated Multi-satellitE Retrievals for GPM (IMERG) technical documentation. *NASA/GSFC Code*, **612**, 2019.

Hunt, J. and Snyder, W. (1980) Experiments on stably and neutrally stratified flow over a model three-dimensional hill. *Journal of Fluid Mechanics*, **96**, 671–704.

Hunt, K. M., Turner, A. G., Stein, T. H., Fletcher, J. K. and Schiemann, R. K. (2021) Modes of coastal precipitation over southwest india and their relationship with intraseasonal variability. *Quarterly Journal of the Royal Meteorological Society*, **147**, 181–201.

India Meteorological Department (2015) Climatological Normals 1981 - 2010. Accessed 28 June 2021, `https://imdpune.gov.in/library/public/`.

Jiang, Q. (2003) Moist dynamics and orographic precipitation. *Tellus A: Dynamic Meteorology and Oceanography*, **55**, 301–316.

Kirshbaum, D. J., Adler, B., Kalthoff, N., Barthlott, C. and Serafin, S. (2018) Moist orographic convection: Physical mechanisms and links to surface-exchange processes. *Atmosphere*, **9**, 80.

Krishna, U. M., Das, S. K., Deshpande, S. M. and Pandithurai, G. (2021) Physical processes controlling the diurnal cycle of convective storms in the Western Ghats. *Scientific Reports*, **11**, 1–13.

Kumar, S. and Bhat, G. (2017) Vertical structure of orographic precipitating clouds observed over south Asia during summer monsoon season. *Journal of Earth System Science*, **126**, 1–12.

Mapes, B. E., Warner, T. T. and Xu, M. (2003) Diurnal patterns of rainfall in northwestern South America. Part III: Diurnal gravity waves and nocturnal convection offshore. *Monthly Weather Review*, **131**, 830–844.

Markowski, P. and Richardson, Y. (2011) Blocking of the Wind by Terrain. In *Mesoscale Meteorology in Midlatitudes*, 343–366. John Wiley & Sons.

Miglietta, M. and Buzzi, A. (2001) A numerical study of moist stratified flows over isolated topography. *Tellus A*, **53**, 481–499.

Miglietta, M. M. and Rotunno, R. (2009) Numerical simulations of conditionally unstable flows over a mountain ridge. *Journal of the Atmospheric Sciences*, **66**, 1865–1885.

Nesbitt, S. W. and Anders, A. M. (2009) Very high resolution precipitation climatologies from the tropical rainfall measuring mission precipitation radar. *Geophysical Research Letters*, **36**.

Nugent, A. D., Smith, R. B. and Minder, J. R. (2014) Wind speed control of tropical orographic convection. *Journal of the Atmospheric Sciences*, **71**, 2695–2712.

Ogura, Y. and Yoshizaki, M. (1988) Numerical study of orographic-convective precipitation over the eastern Arabian Sea and the Ghat Mountains during the summer monsoon. *Journal of the Atmospheric Sciences*, **45**, 2097–2122.

Phadtare, J. (2018) Role of Eastern Ghats orography and cold pool in an extreme rainfall event over Chennai on 1 December 2015. *Monthly Weather Review*, **146**, 943–965.

Pierrehumbert, R. and Wyman, B. (1985) Upstream effects of mesoscale mountains. *Journal of the Atmospheric Sciences*, **42**, 977–1003.

Prabha, T., Goswami, B., Murthy, B. and Kulkarni, J. (2011) Nocturnal low-level jet and 'atmospheric streams' over the rain shadow region of Indian Western Ghats. *Quarterly Journal of the Royal Meteorological Society*, **137**, 1273–1287.

Queney, P. (1948) The problem of air flow over mountains: A summary of theoretical studies. *Bulletin of the American Meteorological Society*, **29**, 16–26.

Rajendran, K., Kitoh, A., Srinivasan, J., Mizuta, R. and Krishnan, R. (2012) Monsoon circulation interaction with Western Ghats orography under changing climate. *Theoretical and Applied Climatology*, **110**, 555–571.

Rani, S. I., Arulalan, T., George, J. P., Rajagopal, E., Renshaw, R., Maycock, A., Barker, D. M. and Rajeevan, M. (2021) IMDAA: High-Resolution Satellite-Era Reanalysis for the Indian Monsoon Region. *Journal of Climate*, **34**, 5109–5133.

Reeves, H. D. and Lin, Y.-L. (2007) The effects of a mountain on the propagation of a preexisting convective system for blocked and unblocked flow regimes. *Journal of the Atmospheric Sciences*, **64**, 2401–2421.

Richardson, H., Basu, S. and Holtslag, A. (2013) Improving stable boundary-layer height estimation using a stability-dependent critical bulk Richardson number. *Boundary-layer meteorology*, **148**, 93–109.

Romatschke, U. and Houze, R. A. (2011) Characteristics of precipitating convective systems in the South Asian monsoon. *Journal of Hydrometeorology*, **12**, 3–26.

Sarker, R. (1966) A dynamical model of orographic rainfall. *Monthly Weather Review*, **94**, 555–572.

Sheppard, P. (1956) Airflow over mountains. *Quarterly Journal of the Royal Meteorological Society*, **82**, 528–529.

Shige, S., Nakano, Y. and Yamamoto, M. K. (2017) Role of orography, diurnal cycle, and intraseasonal oscillation in summer monsoon rainfall over the Western Ghats and Myanmar Coast. *Journal of Climate*, **30**, 9365–9381.

Shrestha, D., Deshar, R. and Nakamura, K. (2015) Characteristics of summer precipitation around the Western Ghats and the Myanmar West Coast. *International Journal of Atmospheric Sciences*, **2015**.

Smith, R. B. (1979) The influence of mountains on the atmosphere. In *Advances in Geophysics*, vol. 21, 87–230. Elsevier.

— (1980) Linear theory of stratified hydrostatic flow past an isolated mountain. *Tellus*, **32**, 348–364.

— (1985) Comment on "Interaction of low-level flow with the Western Ghat Mountains and offshore convection in the summer monsoon. *Monthly Weather Review*, **113**, 2176–2177.

— (1989) Mountain-induced stagnation points in hydrostatic flow. *Tellus A: Dynamic Meteorology and Oceanography*, **41**, 270–274.

Smith, R. B. and Grønås, S. (1993) Stagnation points and bifurcation in 3-D mountain airflow. *Tellus A: Dynamic Meteorology and Oceanography*, **45**, 28–43.

Xie, S.-P., Xu, H., Saji, N., Wang, Y. and Liu, W. T. (2006) Role of narrow mountains in large-scale organization of Asian monsoon convection. *Journal of Climate*, **19**, 3420–3429.

Zhang, G. and Smith, R. B. (2018) Numerical study of physical processes controlling summer precipitation over the Western Ghats region. *Journal of Climate*, **31**, 3099–3115.

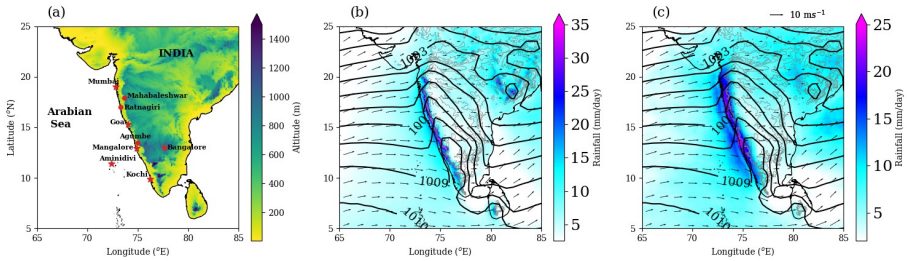

FIGURE 1 (a) Topography of the peninsular India. Radiosonde stations from where the sounding data is used in this study are shown by a star symbol. June-September rainfall accumulations at some of the stations, shown by solid red circles, over the west coast are: Agumbe (659 m): 6866 mm, Mangalore (31 m): 3013 mm, Mahabaleshwar (1382 m) 5362 mm, Ratnagiri (91 m) 2930 mm (India Meteorological Department, 2015). Daily mean June-September rainfall from the (b) IMDAA and (c) IMERG dataset. June-September mean 10m winds and the sea-level pressure (hPa) contours from the ERA-interim dataset are also shown in (b) and (c).

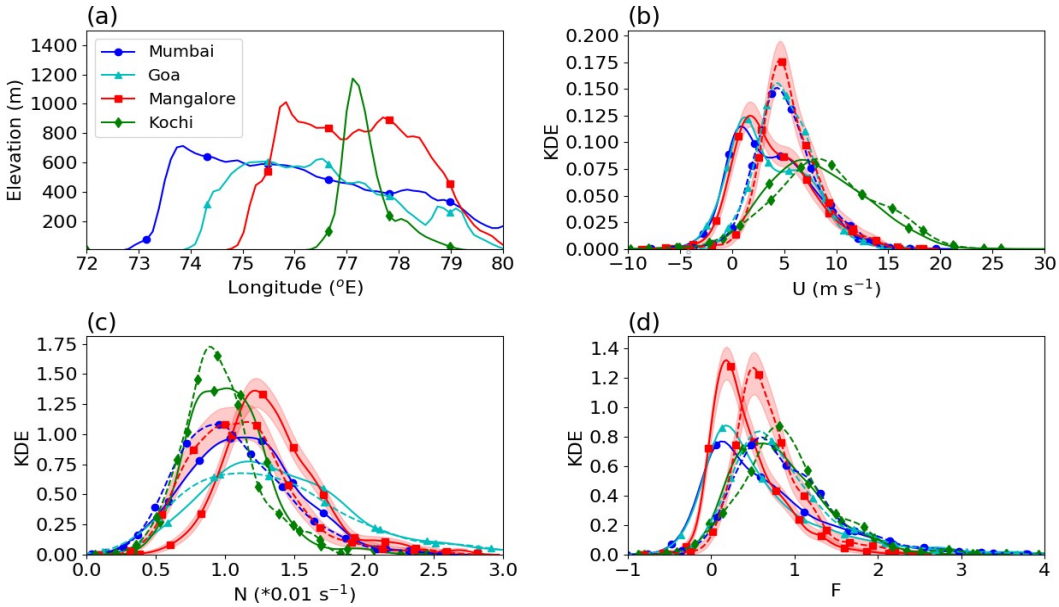

FIGURE 2 (a) Zonal cross-section of orography at each station. Elevation is averaged over 1° latitudinal band centred at the respective radiosonde stations. Kernel density estimation (KDE) of (b) mean zonal winds and (c) mean N over the depths of orography at each station; (d) KDE of F. The solid curves show KDEs from 0000 UTC and the dashed curves show from 1200 UTC soundings. 5-95% confidence interval on the KDE is shown only for Mangalore samples for the sake of clarity.

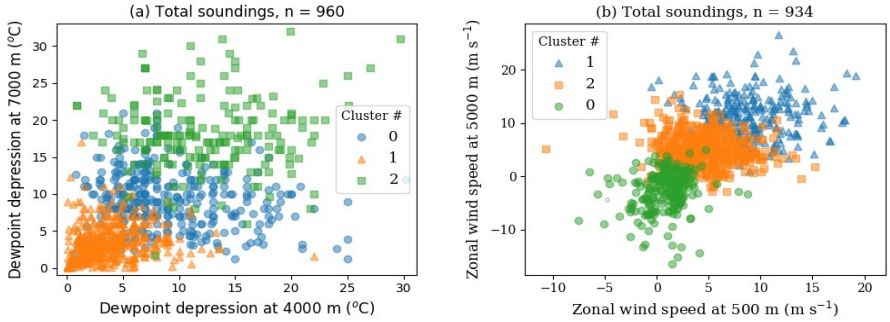

FIGURE 3 (a) Clusters of soundings based on dewpoint depression at 4000, 5000, 6000 and 7000 m. Only values at 4000 and 7000 m are shown in the 2D scatter plot. (b) Clusters of soundings based on the zonal wind speeds at 500, 1000, 2000, 3000, 4000, and 5000 m. Only values at 500 and 5000 m are shown in the 2D scatter plot.

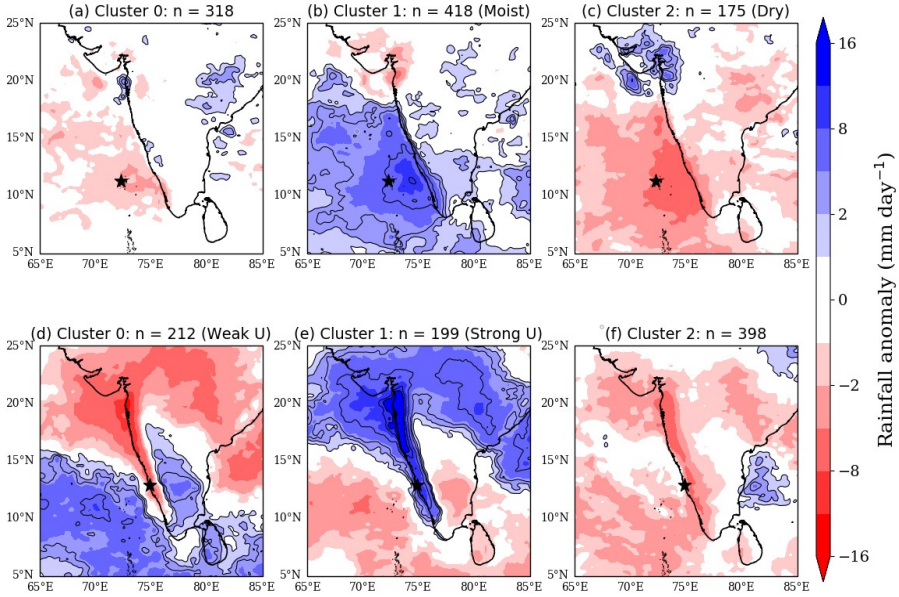

FIGURE 4 Rainfall anomalies (mm day $^{-1}$) in the IMERG dataset for (a) cluster 0, (b) cluster 1, and (c) cluster 2 in Figure 3a; location of Aminidivi is shown by a star. (d), (e), and (f) are same as (a), (b), and (c), respectively, but for the clusters in Figure 3b; location of Mangalore is shown by a star. Thin solid contours show positive rainfall anomalies.

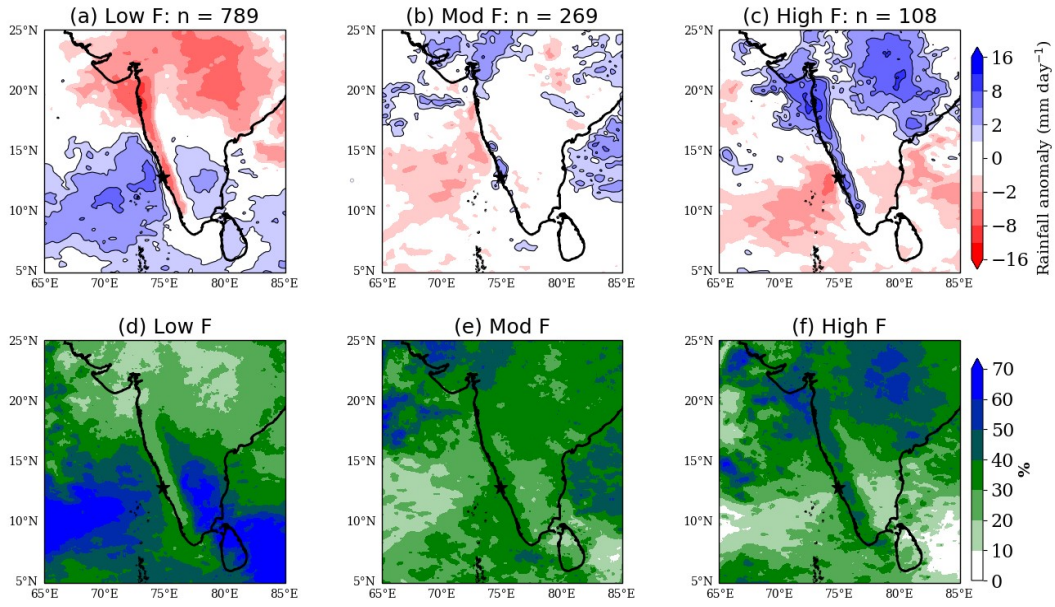

FIGURE 5 Rainfall anomalies (mm day $^{-1}$) in the IMERG dataset during the (a) High, (b) Moderate, and (c) Low *F* phase. Thin solid contours show positive rainfall anomalies. Contribution of (d) High, (e) Moderate, and (f) Low *F* phase to the June-September total rainfall. The phases of *F* are derived from the soundings at Mangalore (location shown by a star).

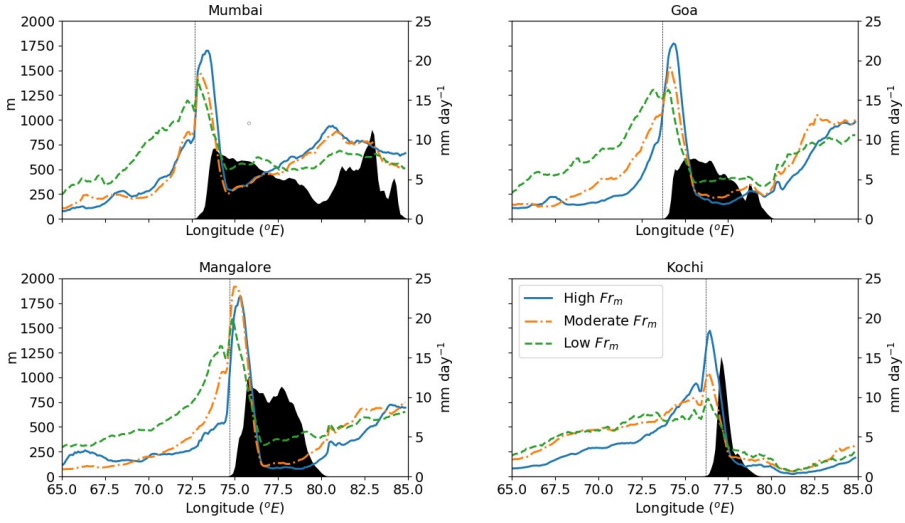

FIGURE 6 Meridional mean of the daily mean rainfall (mm day^{-1}, on the right y-axis) over a 1° latitudinal belt centred at (a) Mumbai, (b) Goa, (c) Mangalore, and (d) Kochi during the three phases of *F* derived from the soundings at the respective stations. The black shading shows the orography with its elevation on the left y-axis.

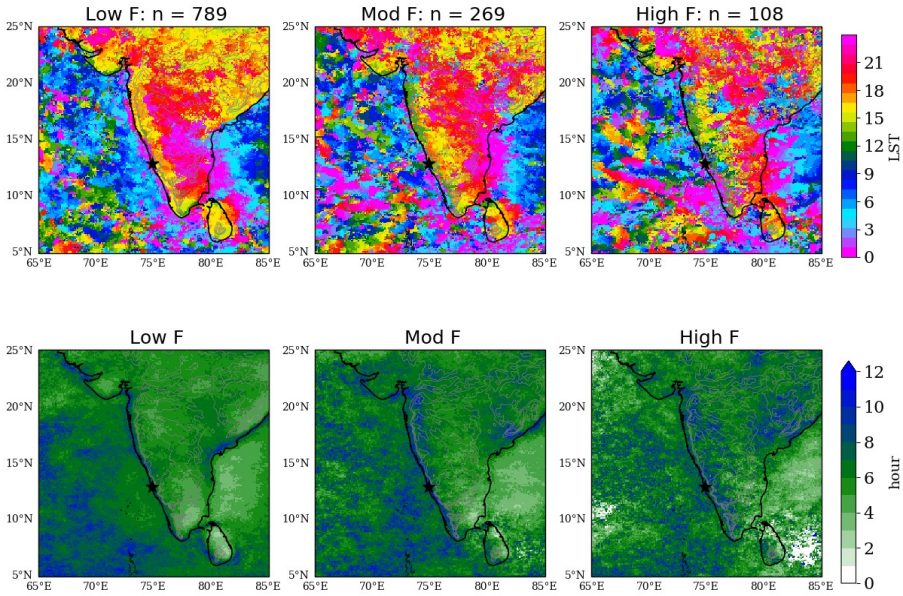

FIGURE 7 Peak of the mean rainfall diurnal cycle in the (a) High, (b) Moderate, and (c) Low *F* phase. Circular standard deviation of the hour of peak rainfall on each day in the (d) High, (e) Moderate, and (f) Low *F* phase. The phases of *F* are derived from the soundings at Mangalore.

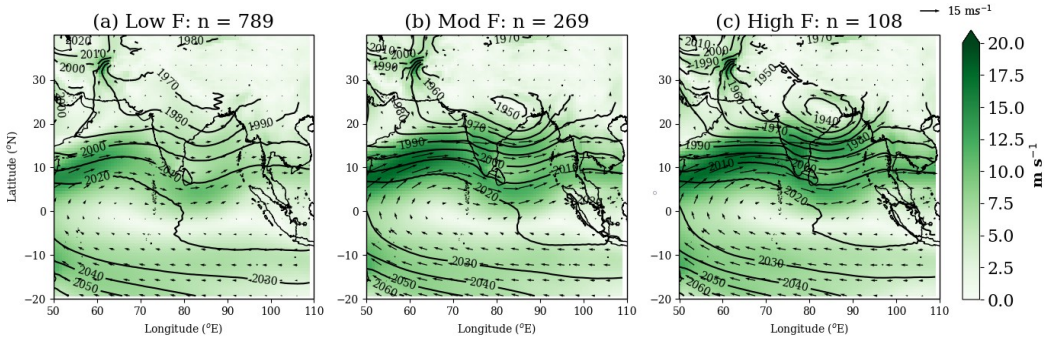

FIGURE 8 800 hPa wind vectors and speed (colour shading) and geopotential height (contour lines) composites for (a) Low, (b) Moderate, (C) High *F* phase derived from the soundings at Mangalore.

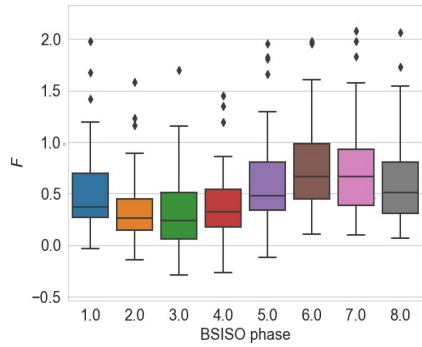

FIGURE 9 Box plots of F values at Mangalore during different BSISO phases.

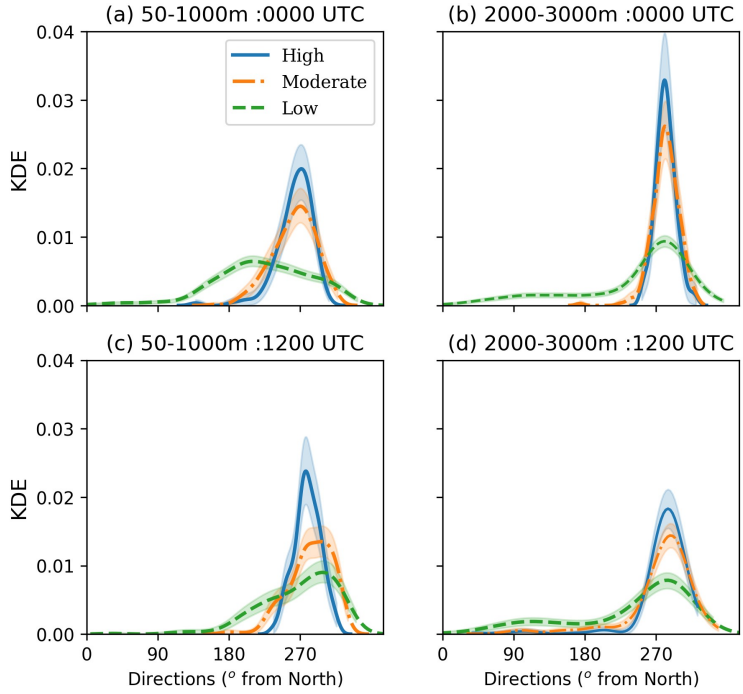

FIGURE 10 KDE of mean wind direction in a layer between (a) 50-1000 m, and (b) 2000-3000 m at Mangalore in the 0000 UTC soundings. (c) Same as (a), and (d) Same as (b) but in the 1200 UTC soundings. Total number of soundings at 0000 UTC: 1545 and at 1200 UTC: 961. The shaded regions show 5-95% confidence intervals for the respective KDEs.

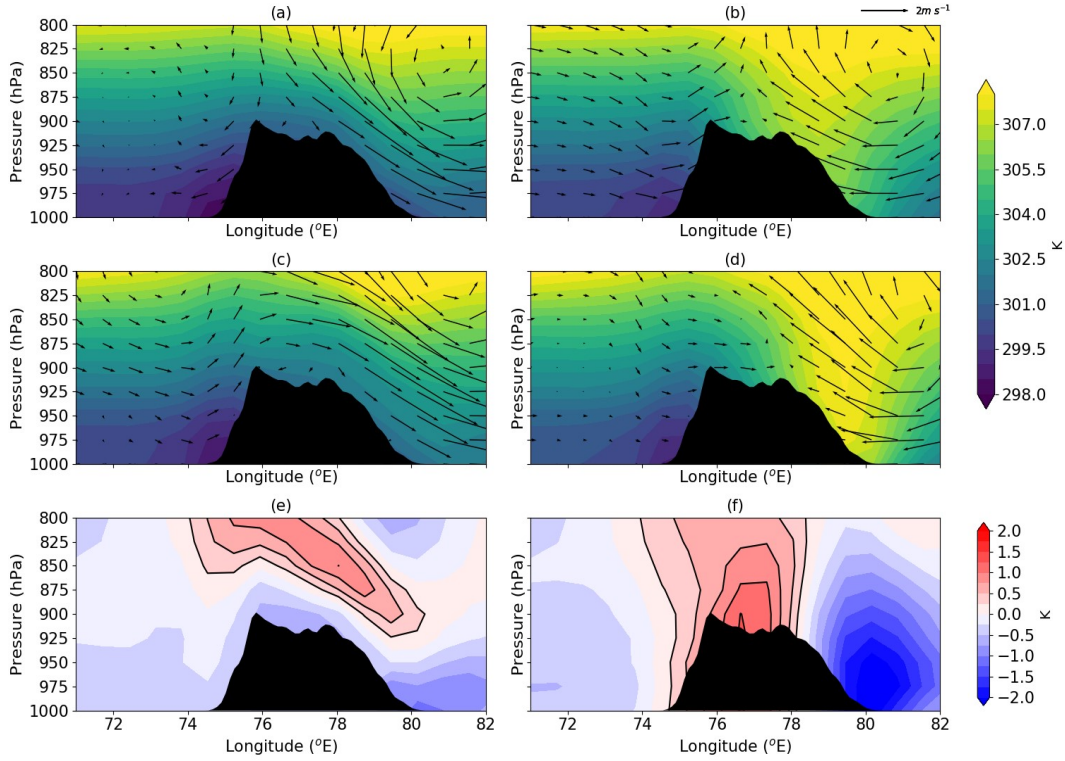

FIGURE 11 12°-14°N mean of the zonal and vertical wind anomalies and potential temperature (θ) from the 0.75° ERA-interim dataset at (a) 0000 UTC and (b) 1200 UTC in the Low F phase. The wind anomalies are derived by subtracting the mean of the Low F phase. (c) Similar to (a), and (d) Similar to (b) but for the High F phase. (e) Difference between θ in (a) and (c), (f) Difference between θ in (b) and (d); the solid contours show positive θ anomalies.

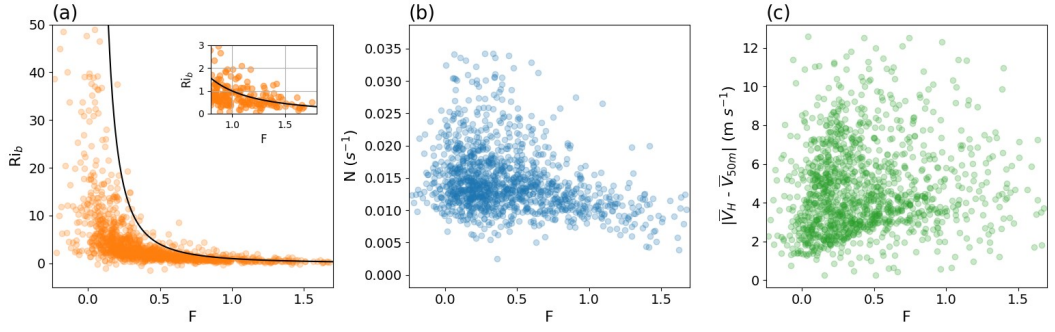

FIGURE 12 Scatter of F versus (a) Ri_b, (b) N, and (c) vertical wind shear ($\overline{V}$ denotes absolute wind velocity) between the mountain top and at 50 m altitude calculated from the 0000 UTC Mangalore soundings. The solid black curve in (a) shows the $Ri_b = 1/F^2$ relation and the inset panel shows the same scatter with a view zoomed over the high F phase.

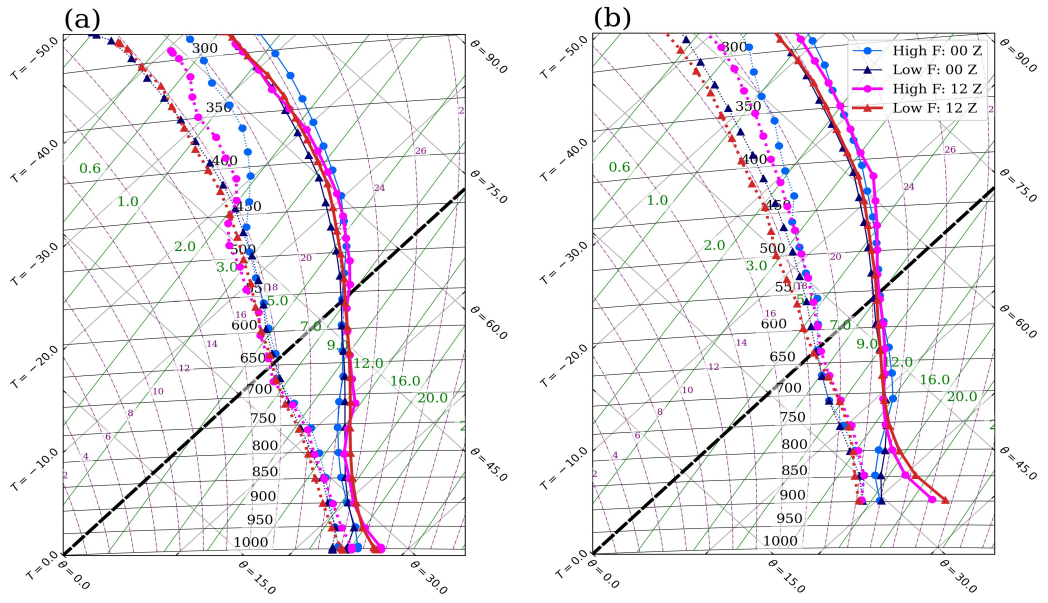

FIGURE 13 Composite 0000 UTC and 1200 UTC soundings in the Low and High *F* phases at (a) Mangalore and (b) Bangalore. The solid line represent dry bulb and the dotted line represent dewpoint temperature profile.

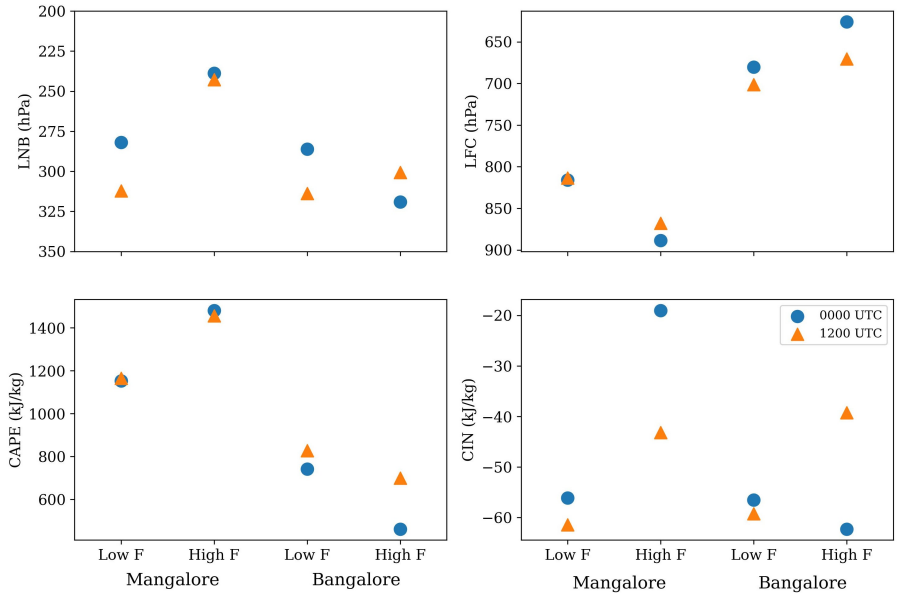

FIGURE 14 Mean (a) LFC, (b) LNB, (c) CAPE, and (d) CIN in the 0000 UTC and 1200 UTC soundings at Mangalore and Bangalore.

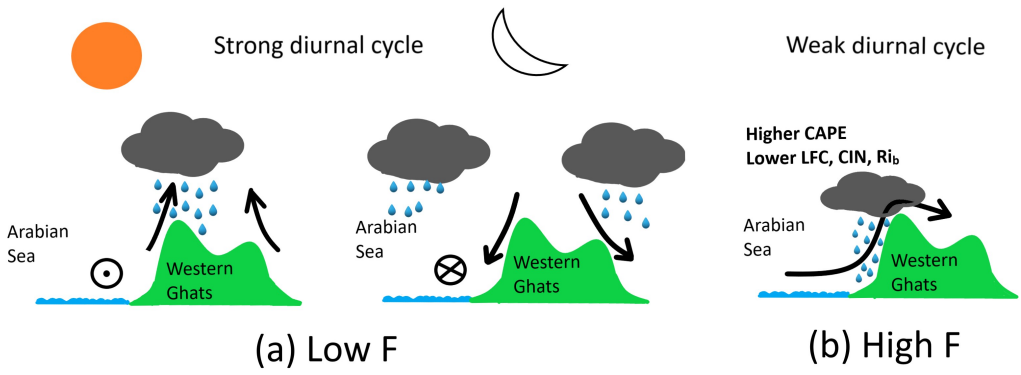

FIGURE 15 (a) Low *F* regime: Characterized by weak onshore winds, occurrences of land-sea/mountain-valley breezes and enhanced rainfall over the offshore and rainshadow (Western Ghats) region in the nocturnal (daytime) hours. Sea (land) breeze over the west coast has a northerly (southerly) component shown by a vector pointing out of (into) the paper. (b) High *F* regime: Characterized by strong onshore winds, absence of land-sea/mountain-valley breezes, higher CAPE and lower LFC, CIN, and Ri_b over the coast and heavy rainfall over the Western Ghats and west coast. Rainfall over the offshore and rainshadow regions is suppressed.